DTU Library

Effect of B+ Flux on the electrical activation of ultra-shallow B+ implants in Ge

Yates, B.R.; Darby, B.L.; Petersen, Dirch Hjorth; Hansen, Ole; Lin, R.; Nielsen, P.F.; Doyle, B.L.; Kontos, A.; Jones, K.S.

Effect of B⁺ Flux on the Electrical Activation of Ultra-Shallow B⁺ Implants in Ge

B. R. Yates[a], B. L. Darby[a], D. H. Petersen[b], O. Hansen[b,d], R. Lin[c], P. F. Nielsen[c], B. L. Doyle[e] , A. Kontos[f], and K. S. Jones[a]

[a] Department of Materials Science and Engineering, University of Florida
Gainesville, Florida 32611, USA

[b] DTU Nanotech, Department of Micro- and Nanotechnology, Technical University of Denmark, DK-2800 Kgs. Lyngby, Denmark

[c] CAPRES A/S, Scion-DTU, DK-2800 Kgs. Lyngby, Denmark

[d] CINF, Center for Individual Nanoparticle Functionality, Technical University of Denmark, DK-2800 Kongens Lyngby, Denmark

[e] Sandia National Laboratories, MS-1056, Albuquerque, NM 87185, United States

[f] Applied Materials, Gloucester, MA 01930

The residual implanted dose of ultra-shallow B⁺ implants in Ge was characterized using elastic recoil detection and was determined to correlate well with simulations with a dose loss of 23% due to ion backscattering for 2 keV implants in Ge. The electrical characterization of ultra-shallow B⁺ implants at 2 keV to a dose of 5.0×10^{14} cm^{-2} at beam currents ranging from 0.4 to 6.4 mA has been studied using micro Hall effect measurements after annealing at 400°C for 60 s. It has been shown that the sheet number increases with beam current across the investigated range with electrical activation being 76% higher at 6.4 mA as compared to 0.4mA. However, at 6.4 mA, the electrically active fraction remained low at 11.4%. Structural characterization revealed that the implanted region remained crystalline and amorphization is not able to explain the increased activation. The results suggest the presence of a stable B:Ge cluster whose formation is altered by point defect recombination during high flux implantation which results in increased B activation.

Introduction

In recent years, the integrated circuit industry has ventured away from the traditional SiO_2/poly-Si gate structure due to physical scaling restraints and has begun using high-κ/metal gate structures which has opened the door to new material choices. Germanium has received a renewed interest as a replacement material for silicon in next-generation metal-oxide semiconductor (MOS) devices due to its increased electron and hole mobility as well as reduced contact resistance. With the renewed interest in Ge, there have been a number of recent reports of electrical activation studies of B⁺ implants in Ge (1-7). In addition, there were a few experiments completed several decades ago (8-10). However,

there is a lack of knowledge regarding ion-implanted dopant incorporation, notably on ultra-shallow B^+ implants. To date, there have been only a few reports regarding the activation behavior of ultra-shallow B^+ implants in Ge (11-14).

For ultra-shallow B^+ implants in Ge, there has been evidence of a B:Ge clustering behavior leading to large fractions of implanted B dose being electrically inactive (13) The behavior is peculiar in that it is independent of implanted dose and occurs in both crystalline (c-Ge) and preamorphized Ge with the clustering behavior far more pronounced in c-Ge samples.   Incomplete activation and B:Ge cluster formation following deep ($\geq$ 35 keV) B^+ implants into crystalline Ge is observed, but the inactive fraction appears to be much more significant with shallow implants (5, 6, 15).

To understand the clustering behavior for ultra-shallow implants in Ge, it is necessary to know the residual chemical dose for a given implant energy. However, the surface proximity increases the difficulty in accurately characterizing the implanted dose using traditional techniques. Elastic recoil detection (ERD) is a viable means for characterizing the implanted dose due to its good depth resolution, its sensitivity to light elements and its ability to measure absolute values without the need for a reference standard.

In an attempt to understand the dopant-defect interactions during implantation and the mechanism behind cluster formation, the effects of varying beam current on the clustering and electrical activation behavior of ultra-shallow B^+ implants in Ge is investigated.

Experimental Methods

Experiments were performed on Czochralski-grown n-type Ge (001) wafers with resistivity greater than 50 Ω-cm. A set of variable beam current samples were diced and B^+-implanted at 2 keV to a dose of 5.0×10^{14} cm^{-2} with beam current varying from 0.4 to 6.4 mA. The beam size is estimated to be 180 cm^2 which yields an ion flux range of 1.38×10^{13} to 2.21×10^{14} ions/(s-cm^2) for 0.4 mA and 6.4 mA, respectively.   During B^+ implantation, the platen was held at 25°C. Samples were processed in a Heatpulse 4100 rapid thermal annealer (RTA) in N_2 ambient at 400°C for 60s to activate the implanted B. High-resolution cross-sectional transmission electron microscopy (HR-XTEM) was completed using a JEOL 2010F to image the microstructure of specimens before and after annealing. TEM samples were prepared using a FEI DB235 focused ion beam.

 Electrical characterization was completed using a a CAPRES microRSP M-150 M4PP with Au-coated probes, a probe spacing of 20 μm, and a permanent magnet with a magnetic flux density of 0.475 T. Hall sheet number (n_H) and mobility values (μ_H) were adjusted to obtain the carrier sheet number (n_s) and drift mobility (μ_d) by using a scattering factor (r_H) of 1.21 as determined empirically by Mirabella et al (1). The carrier density and drift mobility are related to the Hall values by $n_s = n_H \times r_H$ and $\mu_d = \mu_H / r_H$, respectively.

To characterize the as-implanted chemical dose of ultra-shallow B^+ implants in Ge, a set of variable energy samples were implanted at 2, 4, and 6 keV to a dose of 5.0×10^{15} cm^{-2} and characterized using elastic recoil detection (ERD). A dose of 5.0×10^{15} cm^{-2} was used to increase counts and decrease experimentation time. ERD characterization was

performed using the ^{11}B (^{28}Si, ^{11}B) reaction with a 28 MeV Si^{4+} beam with the Ge target tilted at 75˚ from incidence and a recoil angle of 30˚. A 12 μm mylar foil was used to shield forward scattered Si ions and to allow the recoiled B atoms to enter the detector. The areal density of implanted boron was calculated using a spectral scaling approach (16).

Results & Discussion

To confirm the residual implanted dose of ultra-shallow B^{+} implants in Ge, samples implanted to a dose of 5.0×10^{15} cm^{-2} were characterized using ERD. The residual implanted dose for samples implanted at 2, 4, and 6 keV was found to be 3.84×10^{15} cm^{-2}, 3.88×10^{15} cm^{-2}, and 4.12×10^{15} cm^{-2}, respectively. The deviation from the implanted dose is significant as it is in excess of 20% of the implanted dose for the lowest implant energy. As speculated in previous works, it is believed that ion backscatter is a large source of dose loss and at first inspection could seemingly enhance the inactivation of the B^{+} implant (13). Due to the low atomic mass of B in comparison to Ge, it is highly susceptible to ion backscattering during implantation which reduces the chemical dose before any other processing is completed. Taking into account that samples were characterized as- implanted, it is assumed that the deviation from implanted dose is due completely to backscattering losses during implantation. Boron is known to diffuse very slowly in Ge and no further dose loss is expected following annealing at 400˚C for 60s (17, 18).

Fig. 1 shows the percentage of implanted B^{+} lost to backscattering as a function of implant energy as measured with ERD is plotted in conjunction with TRIM simulations (19). The simulations compare favorably with the dose loss values experimentally determined through ERD and confirm that a large portion of the implanted dose is lost to ion backscattering. Given that backscattering is an energy-dependent phenomenon, it is assumed that this behavior is identical for lower doses. The experiment confirms that TRIM simulations are sufficient for estimating the retained implanted dose for ultra-shallow B^{+} implants in Ge.
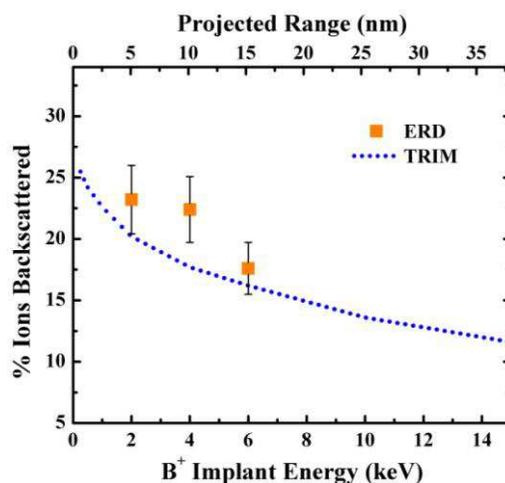

Figure 1. Percent of B ions backscattered as a function of implant energy into Ge as simulated by TRIM and experimentally determined through ERD for a 5.0×10^{15} cm^{-2} implant into Ge.

In Fig 2, the sheet resistance, R_s, is plotted as a function of beam current for 2 keV B$^+$ implants to a dose of 5.0×10^{14} cm^{-2} after annealing 400°C for 60s. A trend of decreasing R_s with increasing beam current is observed across the investigated range. At 6.4 mA, the measured R_s value is 675.2 Ω/sq as compared to 931.5 Ω/sq at 0.4 mA. Interestingly, the decrease in R_s can be explained by an increase in activation as seen in Fig. 3a. At 6.4 mA, the n_s was 4.55×10^{13} cm^{-2} which is an increase of 76% from the lowest current. In Fig. 3b, the drift mobility as a function of beam current is shown. Due to the increase in ionized dopants, the drift mobility decreases with current to a minimum of 203.2 cm^2/V-s which is expected in this doping regime (1).
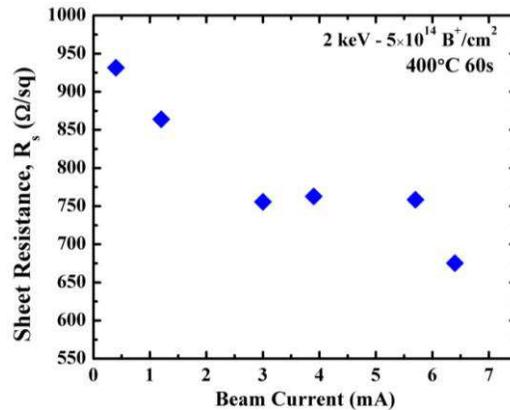

Figure 2. Measured sheet resistance (R_s) after annealing at 400 °C for 60 s as a function of beam current implanted at 2 keV to a dose of 5.0×10^{14} cm^{-2} into crystalline Ge.
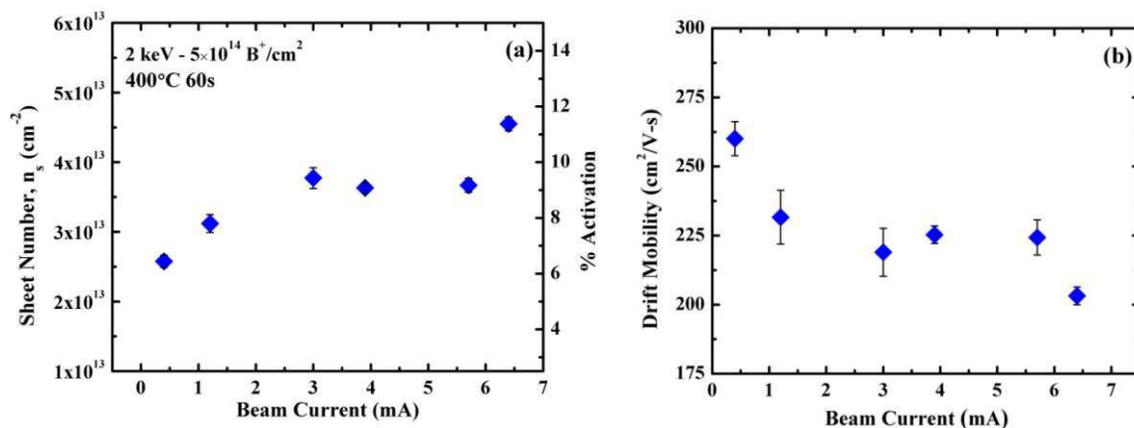

Figure 3. (a) Measured sheet number (n_s) and percent electrical activation and (b) drift mobility (μ_D) as a function of beam current implanted at 2 keV to a dose of 5.0×10^{14} cm^{-2} into crystalline Ge after annealing at 400 °C for 60s.

The microstructure of the samples was characterized using HR-XTEM both as-implanted and post anneal. Fig. 4 shows an image of the 6.4 mA sample in the as-implanted case. The samples implanted at 0.4 and 6.4 mA both appeared unremarkable with no discernible difference between the samples as-implanted and post anneal. The presence of any amorphization was not observed in the as-implanted case and extended defects were not observed in the annealed case for any sample. The lack of

amorphization of the 6.4 mA sample gives credence to the notion that the increased beam current altered the point defect environment during implant which led to the reduction of clustering.
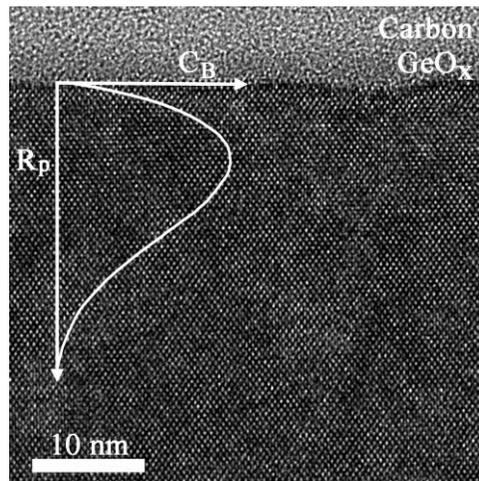

Figure 4. HR-XTEM micrograph of an as-implanted crystalline Ge sample B$^+$ implanted at 2 keV to 5.0×10^{14} cm^{-2} at a beam current of 6.4 mA showing a 2.9 ± 0.3 nm surface GeO$_x$ layer and no evident implant damage or amorphization present near the projected range, R_p. A simulation of the B profile is overlaid on the image.

Despite the increase in carriers with increasing beam current, the overall activation of the samples is far from complete activated with the highest value achieved at 11.4%; where the active fraction is simply the sheet number divided by the residual dose as simulated by TRIM. This finding is not surprising given the recent report of an anomalous clustering behavior in Ge which had reported ~10% activation for 2 keV B$^+$ implanted at doses ranging from 5.0×10^{13} cm^{-2} to 5.0×10^{15} cm^{-2} (13). Previous reports have reported incomplete activation for higher energy implants in Ge and have attributed it to B:Ge cluster formation (5, 6, 15).

It should be noted that the observed increase in active carriers is not believed to be due to any beam heating effects due to the platen being held at room temperature during the implantation. For Si, it is well-known that varying the beam current during implantation can significantly alter the resulting microstructure through ion beam induced recrystallization or amorphization (20, 21). At elevated temperatures, a subtle change in the ion flux is capable of influencing the point defect environment surrounding the crystalline-amorphous interface in such a way that it may recrystallize or further amorphize the layer depending on an increase or decrease in beam current, respectively. Several studies regarding ion beam induced recrystallization and amorphization have been completed with Ge which have reported similar findings (22-24). Notably, Sigurd et al. have reported that for B ions in Ge, the lattice disorder produced is ten times higher than what is observed in Si at room temperature (22). These results are likely explained through the lower amorphization threshold of Ge as compared to Si (25). However, for light ions such as B, the amorphous layer is not as thick nor is amorphization observed at the projected range of the ion as predicted by simulations for heavier ions, but rather occurs closer to the surface (26). The dilute damage cascades created by light ions allow Frenkel pairs created during implantation to recombine or to form larger, stable

complexes such as a B:Ge cluster. Therefore, by increasing the beam current during implantation, the point defect environment is altered which allows for a reduction in the formation of B:Ge clusters.

Conclusions

The residual implanted dose for ultra-shallow B^+ implants in Ge was characterized using ERD and compare favorably with simulations suggesting a dose loss due to backscattering of 23%. Samples implanted at 2 keV to a dose of 5.0×10^{14} cm^{-2} at varying ion beam current were characterized using micro four point probe and micro Hall effect techniques. The results show a decrease in R_s with increasing beam current due to an increase in electrical activation. However, despite the increase in activation, the highest sheet number obtained was 4.55×10^{13} cm^{-2} which corresponds to a maximum active fraction of 11.4%. HR-XTEM characterization showed no discernible microstructural difference between samples. The results suggest a B:Ge cluster formation that is altered through a change in the point defect environment with increased beam current during implantation.

Acknowledgments

References

1. S. Mirabella, G. Impellizzeri, A.M. Piro, E. Bruno, and M.G. Grimaldi, *Appl. Phys. Lett*., **92**, 251909 (2008).
2. Y.-L. Chao, S. Prussin, J.C.S. Woo, and R. Scholz, *Appl. Phys. Lett.,* **87**, 142102 (2005).
3. Yu-Lin Chao and J.C.S. Woo, Electron Devices, *IEEE Transactions* **54**, 2750–2755 (2007).
4. Y.S. Suh, M.S. Carroll, R.A. Levy, M.A. Sahiner, G. Bisognin, and C.A. King, *IEEE Transactions On,* **52**, 91– 98 (2005).
5. Yong Seok Suh, M.S. Carroll, R.A. Levy, G. Bisognin, D. De Salvador, M.A. Sahiner, and C.A. King, *IEEE Transactions On* **52**, 2416–2421 (2005).
6. G. Impellizzeri, S. Mirabella, E. Bruno, A.M. Piro, and M.G. Grimaldi, *J. Appl. Phys,.* **105**, 063533 (2009).
7. F. Panciera, P.F. Fazzini, M. Collet, J. Boucher, E. Bedel, and F. Cristiano, *Appl. Phys. Lett.,* **97**, 012105 (2010).
8. K.S. Jones and E.E. Haller, *J. of Appl. Phys.,* **61**, 7 (1987).
9. V.M. Gusev, M.I. Guseva, E.S. Ionova, A.N. Mansurova, and C.V. Starinin, *Phys. Stat. Sol,.* **21**, 413–418 (1974).
10. M.I. Guseva and A.N. Mansurova, *Radiation Effects*, **20**, 207–210 (1973).
11 A. Satta, E. Simoen, T. Clarysse, T. Janssens, A. Benedetti, B. De Jaeger, M. Meuris, and W. Vandervorst, *Appl. Phys. Lett*., **87**, 172109 (2005).

12.   E. Simoen, G. Brouwers, A. Satta, M.-L. David, F. Pailloux, B. Parmentier, T. Clarysse, J. Goossens, W. Vandervorst, and M. Meuris, *Mat. Sci. in Semicon. Process.,* **11**, 368–371 (2008).

13.   B.R. Yates, B.L. Darby, N.G. Rudawski, K.S. Jones, D.H. Petersen, O. Hansen, R. Lin, P.F. Nielsen, and A. Kontos, *Mater. Lett.,* **65**, 3540–3543 (2011).

14.   G. Hellings, E. Rosseel, T. Clarysse, D.H. Petersen, O. Hansen, P.F. Nielsen, E. Simoen, G. Eneman, B. De Jaeger, T. Hoffmann, K. De Meyer, and W. Vandervorst, Microelectronic Engineering **88**, 347–350 (2011).

15.   G. Bisognin, S. Vangelista, M. Berti, G. Impellizzeri, and M.G. Grimaldi, *J. Appl. Phys.*, **107**, 103512 (2010).

16.   B.L. Doyle and D.K. Brice, *Nucl. Instrum. Methods Phys. Res. B*, **35**, 301–308 (1988).

17.   S. Uppal, A.F.W. Willoughby, J.M. Bonar, A.G.R. Evans, N.E.B. Cowern, R. Morris, and M.G. Dowsett, *J. Appl. Phys.*, **90**, 4293 (2001).

18.   S. Uppal, A.F.W. Willoughby, J.M. Bonar, N.E.B. Cowern, T. Grasby, R.J.H. Morris, and M.G. Dowsett, *J. Appl. Phys.*, **96**, 1376–1380 (2004).

19.   J.F. Ziegler, *Nucl. Instrum. Methods Phys. Res. B*, **219-220**, 1027–1036 (2004).

20.   R.G. Elliman, J.S. Williams, W.L. Brown, A. Leiberich, D.M. Maher, and R.V. Knoell, *Nucl. Instrum. Methods Phys. Res. B*, **19–20, Part 2**, 435–442 (1987).

21.   R.G. Elliman, S.T. Johnson, A.P. Pogany, and J.S. Williams, *Nucl. Instrum. Methods Phys. Res. B*, **7–8,** 310–315 (1985).

22.   D. Sigurd, G. Fladda, L. Eriksson, and K. Björkqvist, *Radiation Effects*, **3**, 145–147 (1970).

23.   G. Holmén, S. Peterström, A. Burén, and E. B⊘gh, *Radiation Effects*, **24**, 45–50 (1975).

24.   J. Linnros and G. Holmén, *J. of Appl. Phys.,* **62**, 4737–4744 (1987).

25   S. Koffel, P. Scheiblin, A. Claverie, and G. Benassayag, *J. of Appl. Phys.,* **105**, 013528 (2009).

26.   A. Claverie, S. Koffel, N. Cherkashin, G. Benassayag, and P. Scheiblin, *Thin Solid Films*, **518**, 2307–2313 (2010).